

## In Situ UV Raman Spectroscopic Studies on the Synthesis Mechanism of Zeolite X

Fengtao Fan,<sup>[a, b]</sup> Zhaochi Feng,<sup>[a]</sup> Guanna Li,<sup>[a, b]</sup> Keju Sun,<sup>[a, b]</sup> Pinliang Ying,<sup>[a]</sup> and Can Li<sup>\*[a]</sup>

Microporous materials, often referred to as molecular sieves or open-framework materials, are a class of inorganic solids that possess regular pores or voids in the size range of 5–20 Å. Zeolites are the most well known family of such materials.<sup>[1,2]</sup> Even though numerous zeolite structures have been successfully synthesized, it is still necessary to rationally design and synthesize more and more zeolite structures with specific architectures and properties, which requires a full understanding of the crystallization process and the formation mechanism of zeolites.<sup>[3]</sup> Various mechanisms have been discussed regarding the process of establishing the long-range crystal structure.<sup>[4–9]</sup> Several assembly mechanisms regarding the nucleation and crystal growth have been proposed, including the formation and consumption of small primary units, medium nuclei, and large crystals.<sup>[10]</sup> Despite these efforts, due to the complexity of the zeolite formation process, a thorough understanding of the zeolite formation mechanism remains a challenge.<sup>[11]</sup>

Many techniques, such as X-ray diffraction and scattering,<sup>[12]</sup> NMR spectroscopy,<sup>[13]</sup> and electron microscopy<sup>[14]</sup> have been used to study the formation mechanism of zeolites. Most studies were performed by using *ex situ* techniques, namely by frequently removing aliquots of the reaction mixture and analyzing the samples after quenching the reaction. However, microporous zeolite-type materials are usually synthesized under hydrothermal conditions, and the need for sample quenching and workup may cause dramatic and undeterminable structural changes.<sup>[15]</sup> Moreover, it is

very difficult to follow the complex mechanism by which they assemble from precursor species.<sup>[16]</sup>


In situ real-time characterization that can probe the intermediate species occurring during zeolite formation, without the need for quenching, not only allows the continuous monitoring of the reaction, but also allows the reactions to be studied under real reaction conditions. Thus, it is paramount to study the synthesis mechanism of zeolites under actual synthesis conditions, by developing in situ characterization methods.<sup>[17–19]</sup>

Raman spectroscopy is a suitable technique to investigate aqueous solutions as well as solid phases of zeolite synthesis mixtures due to the low Raman scattering cross section of water. In situ visible Raman spectroscopy has been shown to be suitable for monitoring the evolution of the template during the hydrothermal synthesis.<sup>[20]</sup> However, it is often not possible to use visible Raman spectroscopy to monitor the zeolite framework formation due to the strong fluorescence caused by the template and highly hydrated material during the hydrothermal process. In particular, UV Raman spectroscopy has been demonstrated to be a powerful tool for the characterization of zeolites with its advantages of avoiding the fluorescence and increasing the sensitivity.<sup>[21,22]</sup> These advantages make UV Raman spectroscopy a potentially valuable tool for the in situ study of the mechanism of zeolite framework formation.

Herein we demonstrate that UV Raman techniques can be applied to the in situ study of zeolite synthesis and are suitable for monitoring the formation and evolution of intermediate species under hydrothermal synthesis conditions. In the present work, we monitor the evolution of precursors and the formation of zeolite crystal particles during the hydrothermal crystallization of zeolite X, using a specially designed in situ Raman cell coupled to a UV Raman spectrometer. A formation mechanism of zeolite X in both the liquid and solid phase is presented based on the Raman results combined with X-ray diffraction patterns,<sup>[27]</sup> Al MAS NMR spectroscopy, and theoretical calculations.

[a] F. Fan, Prof. Dr. Z. Feng, G. Li, K. Sun, Dr. P. Ying, Prof. Dr. C. Li  
State Key Laboratory of Catalysis  
Dalian Institute of Chemical Physics  
Chinese Academy of Sciences  
457 Zhongshan Road, Dalian, 116023 (China)  
Fax: (+86) 411-84694447  
E-mail: canli@dicp.ac.cn

[b] F. Fan, G. Li, K. Sun  
Graduate School of the Chinese Academy of Sciences (China)

 Supporting information for this article is available on the WWW under <http://www.chemistry.org> or from the author.

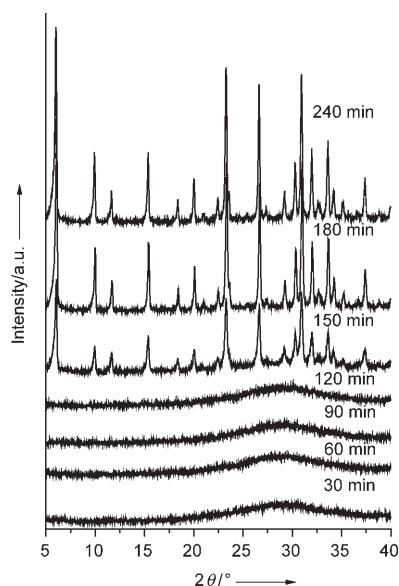


Figure 1. Powder X-ray diffraction patterns of the solid phase of zeolite X formed after crystallization for 30, 60, 90, 120, 150, 180, and 240 min.

Figure 1 shows the powder X-ray diffraction patterns of the solid phase of zeolite X for the various stages of crystallization. The X-ray diffraction patterns after the crystallization for 30, 60, 90, and 120 min show only the peaks of the amorphous aluminosilicate solids. The peaks at 6.1, 10.0, 15.4, 23.3, 26.6, and 30.9 are observed in the XRD patterns of the samples after a crystallization for 150 min. These peaks are characteristic of zeolites with a FAU structure. Highly crystalline zeolite X was obtained after a crystallization for 180 min.

Figure 2 shows the in situ Raman cell for the hydrothermal synthesis of zeolites. The cell is designed to simulate the real synthesis autoclave that operates under high pressure and temperature. It is surrounded by a copper heating loop. A lens was sealed with silicon rubber on the top of the cell to focus the laser on the surface of the studied samples in the cell. By using a lens as the window of the in situ cell, the Raman signal is more than 3–4 times stronger than that obtained using a plane window. It can withstand temperatures up to 250°C and a pressure of about 40 bar under hydrothermal conditions for zeolite synthesis. To investigate the

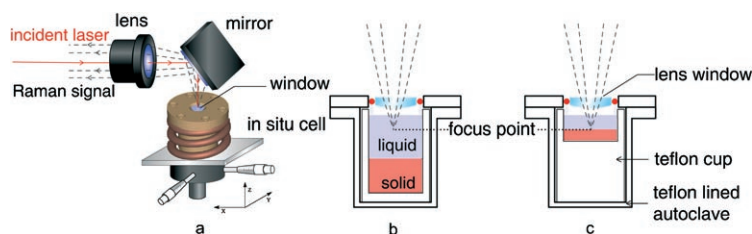


Figure 2. Schematic diagram of a) the in situ Raman cell for hydrothermal synthesis of zeolites, b) the sample holder inserted into the in situ Raman cell for the liquid-phase study and the focus point, and c) the sample holder inserted into the in situ Raman cell for the solid-phase study and the focus point.

synthesis reactions in the liquid and solid phases, two types of sample holders were used. For the liquid phase, we used a deep cup to focus the laser in the liquid layer (Figure 2b). For the solid phase, we used a shallow cup so that the laser point can be focused on the interface between the liquid and solid phases (Figure 2c).

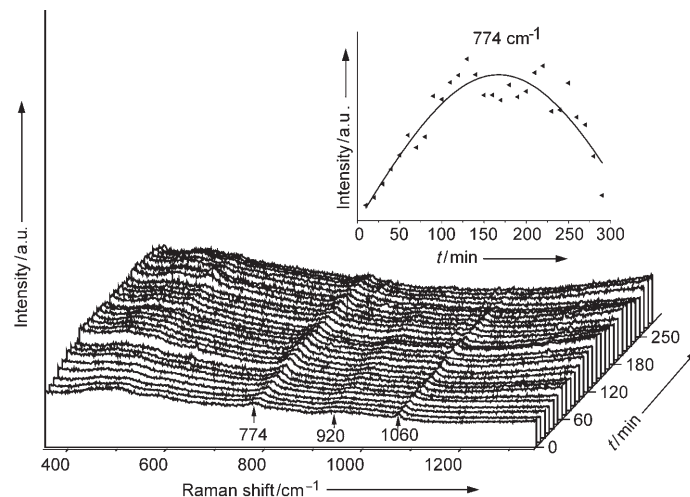


Figure 3. In situ UV Raman spectra (excited at 325 nm) of the liquid phase of zeolite X synthesis at 373 K; spectra were collected from 0 min to 270 min, at intervals of 15 min. Insert: Plot of the intensity of the band at 774  $\text{cm}^{-1}$  as a function of crystallization time.

Figure 3 shows in situ UV Raman spectra recorded for the liquid phase at 373 K under hydrothermal conditions. The initial spectrum of the liquid phase presents a broad band centered at 500  $\text{cm}^{-1}$ , and distinct bands at 774, 920, and 1060  $\text{cm}^{-1}$ . The band at 500  $\text{cm}^{-1}$  is attributed to amorphous silicate. The band at 1060  $\text{cm}^{-1}$  is associated with  $\text{CO}_3^{2-}$  species formed in the gel due to the reaction of NaOH and  $\text{CO}_2$  in solution.<sup>[23]</sup> The bands at 774 and 920  $\text{cm}^{-1}$  appear and vary in parallel steps. The two bands can be attributed to monomeric silicate species in the liquid phase.<sup>[24–26]</sup> A plot of the intensity of the band at 774  $\text{cm}^{-1}$  as a function of time is shown in the insert of Figure 3. The intensity of the band at 774  $\text{cm}^{-1}$  increases with crystallization time and reaches a maximum intensity at about 120 min, and then decreases on prolonged crystallization time. This indicates that the liquid phase is dominated by monomeric silicate species that are directly involved in the zeolite formation. This process can be described as follows: In the initial gel, the amorphous solid is in equilibrium with solution species. With increasing temperature, a large amount of monomers are formed from the depolymerization of amorphous precursors

(see Figure 1, 30–90 min). As the reaction proceeds, the growing product crystals (see Figure 1, 90–180 min) require more monomers. Finally, all amorphous precursors have been consumed and transformed into the crystalline zeolite (see Figure 1, 180–240 min).

The sharp band at  $500\text{ cm}^{-1}$  in Figure 4 indicates that the gel predominantly consists of 4-rings.<sup>[27,28]</sup> Upon heating, this band becomes prominent, and gradually shifts to  $514\text{ cm}^{-1}$ , which is the breathing mode vibration of the 4-ring in the crystalline framework of zeolite X. The characteristic Raman bands of zeolite X at  $298$  and  $380\text{ cm}^{-1}$  appear with the development of the synthesis. These bands, which are assigned to the bending mode of double 6-rings, indicate that the formation of zeolite X framework is directly related to the 4-ring and 6-ring species.<sup>[29]</sup> A plot of the intensity of the band at  $514\text{ cm}^{-1}$  is shown in the insert of Figure 4. Significant changes in the intensity of this band are observed after heating for 150 min. This is in accordance with the X-ray diffraction results (see Figure 1).

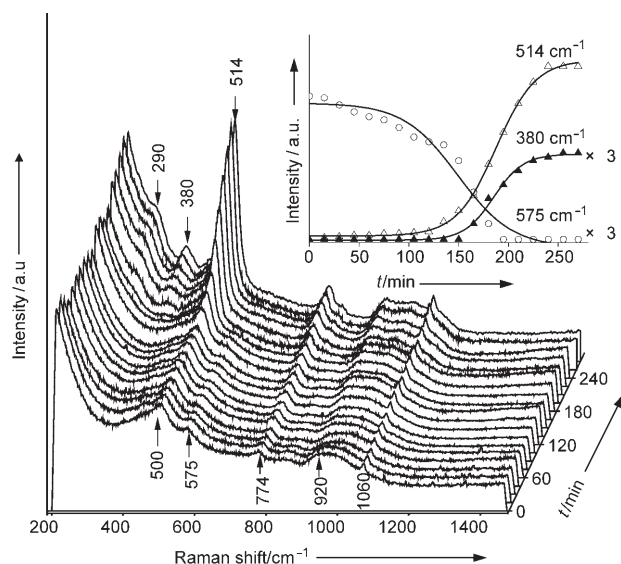


Figure 4. In situ UV Raman spectra (excited at  $325\text{ nm}$ ) of the solid phase of zeolite X synthesis at  $373\text{ K}$ ; spectra were collected from  $0\text{ min}$  to  $270\text{ min}$ , at intervals of  $10\text{ min}$ . Insert: Plot of intensities of the bands at  $380$ ,  $514$ , and  $575\text{ cm}^{-1}$  as a function of crystallization time.

It is noteworthy that the band at  $575\text{ cm}^{-1}$  appears at the very beginning of the synthesis. This band is attributed to the aluminosilicate precursors, and diminishes during the crystallization (see insert of Figure 4). The most interesting phenomenon is that two bands at  $298$  and  $380\text{ cm}^{-1}$  appear, while the band at  $575\text{ cm}^{-1}$  disappears, indicating that the band at  $575\text{ cm}^{-1}$  is directly related to the formation of the framework of zeolite X. Clearly, the species giving rise to the band at  $575\text{ cm}^{-1}$  is a key intermediate in the formation of zeolite X. Raman bands between  $550$  and  $600\text{ cm}^{-1}$  have been assigned to Al-O-Si stretches.<sup>[30]</sup> Guth et al. reported a band at  $577\text{ cm}^{-1}$  for a solution of aluminate and silicate

under strong basic conditions, and assigned the band to the aluminosilicate anions.<sup>[25]</sup> Dutta et al. also observed this band in similar aluminosilicate solutions.<sup>[31]</sup>

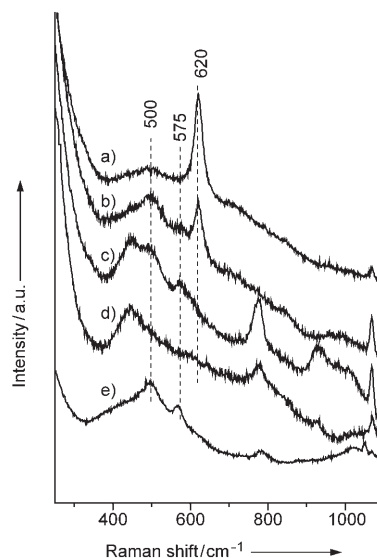


Figure 5. UV Raman spectra of the gel phase a)  $\text{SiO}_2/\text{Al}_2\text{O}_3=1:1$ ; b)  $\text{SiO}_2/\text{Al}_2\text{O}_3=2:1$ ; c)  $\text{SiO}_2/\text{Al}_2\text{O}_3=4:1$ ; d) the liquid phase  $\text{SiO}_2/\text{Al}_2\text{O}_3=4:1$ ; and e) the solid phase  $\text{SiO}_2/\text{Al}_2\text{O}_3=4:1$  after washing with water.

Figure 5a–c show the UV Raman spectra of a series of gels with similar composition but different  $\text{SiO}_2/\text{Al}_2\text{O}_3$  ratios. The intensity of the band at  $575\text{ cm}^{-1}$  increases together with that at  $500\text{ cm}^{-1}$ , which is due to the ring breathing vibration of the 4-ring. In addition, the band at  $575\text{ cm}^{-1}$  is detected in the Raman spectrum of the solid phase of the gel with a  $\text{SiO}_2/\text{Al}_2\text{O}_3$  ratio of  $4:1$  (Figure 5e), whereas the band at  $575\text{ cm}^{-1}$  is not observed in the Raman spectrum of the liquid phase of the gel with a  $\text{SiO}_2/\text{Al}_2\text{O}_3$  ratio of  $4:1$  (Figure 5d), indicating that the band at  $575\text{ cm}^{-1}$  is associated with the solid phase of the precursor (Figure 5c–e). These results suggest that the band at  $575\text{ cm}^{-1}$  may be related to the Al-O-Si unit associated with the ring structure in the precursor. The fact that this vibration shows a very different frequency compared to that of the Al-O-Si unit in the ring structures suggests that this band may mainly originate from a ring with branched chains.<sup>[25]</sup>

The mechanism of the formation of the framework of zeolite X, based on in situ Raman spectra and DFT calculations, is proposed in Figure 6: In the very early stage of the synthesis process, the amorphous precursor (“gel”) is dissolved to yield small soluble species such as monomer silicate species that are characterized by the increase of the band intensity at  $774\text{ cm}^{-1}$ . The precursors are dominated by 4-ring structures, although some of them may possibly exist in a branched form, which is characterized by the band at  $575\text{ cm}^{-1}$ . The 4-rings connect with each other to form fragments<sup>[10]</sup>—a process that is characterized by an increase of the band intensity around  $500\text{ cm}^{-1}$  and a decrease of the band intensity at  $575\text{ cm}^{-1}$ . This period is the well-known

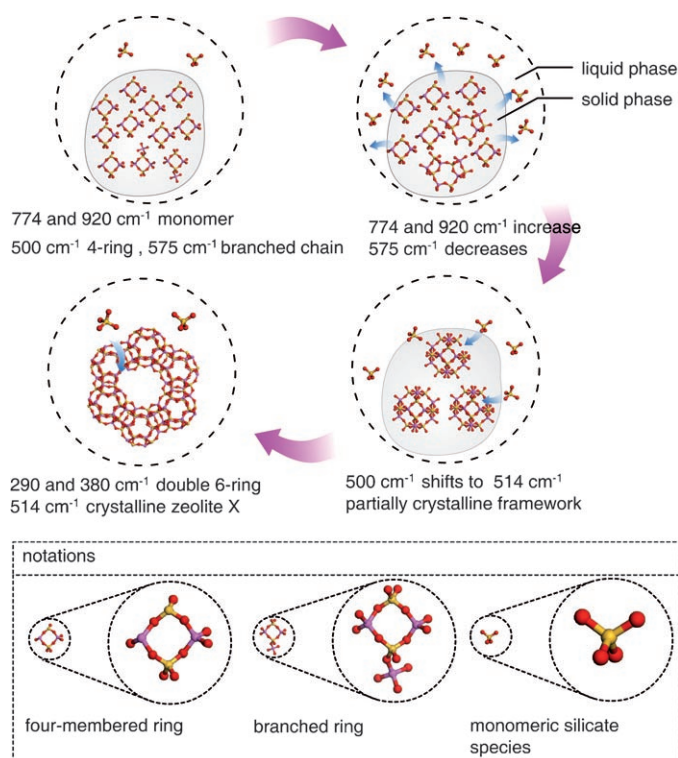


Figure 6. A proposed mechanism for the synthesis of the framework of zeolite X.

“induction period” in zeolite synthesis, which is a “black” stage in terms of XRD patterns, but can be characterized by UV Raman spectroscopy. During this stage, the monomer species are concentrated and become involved in the formation of the framework of zeolite X, a process that is accompanied by a decrease in the band intensity at  $774\text{ cm}^{-1}$  in the liquid phase and an increase in the intensity of the band due to the zeolite formation in the solid phase. The gradual shift of the band at  $500$  to  $514\text{ cm}^{-1}$  indicated that some partially crystalline domains may form.<sup>[9]</sup> The appearance of the bands of double 6-rings and a 4-ring at  $514$ ,  $290$ , and  $380\text{ cm}^{-1}$  indicates the formation of the finely crystalline framework by the conversion of partially crystalline domains by aggregation and realignment of preassembled building blocks.<sup>[9,10,33]</sup> Most of the precursors become crystalline at the end of the crystallization, while the monomers are consumed. This is in agreement with the drop in intensity of the monomer species at  $774\text{ cm}^{-1}$  in the liquid phase.

In summary, in situ UV Raman spectroscopy is demonstrated to be a powerful tool for monitoring the solid and liquid phases in zeolite synthesis under hydrothermal conditions. During the hydrothermal synthesis of zeolite X, the amorphous solid phase dissolves to form monomer silicate species in the liquid phase, while amorphous aluminosilicate species composed of predominately 4-rings are formed in the solid phase in the early stage of nucleation. These 4-rings are connected with each other via double 6-rings together with the monomer silicate species in the liquid phase to form the crystalline zeolite X framework. In situ Raman

spectroscopy could be applied to the study of the synthesis mechanisms of a wide range of zeolites as well as many other materials, particularly in hydrothermal synthesis at high pressures and temperatures.

## Experimental Section

**Synthesis procedure of zeolite X:** The starting composition of the seed solution for zeolite X synthesis is  $18\text{Na}_2\text{O}\cdot 1\text{Al}_2\text{O}_3\cdot 19\text{SiO}_2\cdot 370\text{H}_2\text{O}$ . The seed solution was prepared and then aged at room temperature for 24 h. The final seed solution is a clean solution. The composition of the starting gel is  $3\text{Na}_2\text{O}\cdot 1\text{Al}_2\text{O}_3\cdot 3\text{SiO}_2\cdot 117\text{H}_2\text{O}$ . Sodium silicate was added to the solution of sodium aluminate in NaOH. The seed solution was added to the solution when the hydrolysis of the reaction mixture was finished. The reaction mixture was stirred rapidly to form a homogeneous gel with a Si/Al ratio of 1.5:1.

**Characterization:** UV Raman spectra were measured with a Jobin–Yvon T64000 triple-stage spectrometer with spectral resolution of  $2\text{ cm}^{-1}$ . The laser line at  $325\text{ nm}$  of a He/Cd laser was used as an exciting source with an output of  $50\text{ mW}$ . The power of the laser at the sample was about  $3.0\text{ mW}$ .

**Theoretical methods:** DFT, with the B3LYP hybrid exchange–correlation functional, was used to perform the calculations. Geometry optimizations were all performed with the Gaussian 03 program, and a 6-31+G(d,p) basis set was used. For all the systems considered we have determined equilibrium geometries in the gas phase and have evaluated vibrational frequencies. To allow a comparison with the experimental results, all the computed frequencies were scaled by a factor of 0.96 to account for the overbinding of the exchange–correlation functional employed in density functional theory. The solvation effect was included by using the continuum solvation COSMO method implemented in the Gaussian 03 package. The COSMO method has been reported to be an appropriate approach for studying the silica reaction in a solution.<sup>[33–35]</sup>

## Acknowledgements

This work was financially supported by the National Basic Research Program of China (2003CB615806, 2004CB720607, 2005CB221407) and the National Natural Science Foundation of China (20773118, 20673115).

**Keywords:** hydrothermal synthesis • Raman spectroscopy • reaction mechanisms • UV spectroscopy • zeolites

- [1] R. M. Barrer, *Hydrothermal Chemistry of Zeolites*, Academic Press, London **1982**.
- [2] M. E. Davis, R. F. Lobo, *Chem. Mater.* **1992**, *4*, 756–768.
- [3] R. R. Xu, W. Q. Pang, J. H. Yu, Q. S. Huo, J. S. Chen, *Chemistry of Zeolites and Related Porous Materials*, Wiley, New York, **2007**.
- [4] C. S. Cundy, M. S. Henty, R. J. Plaisted, *Zeolites* **1995**, *15*, 342–352.
- [5] a) S. L. Burkett, M. E. Davis, *J. Phys. Chem.* **1994**, *98*, 4647–4653; b) M. Tsapatsis, M. Lovallo, M. E. Davis, *Microporous Mater.* **1996**, *5*, 381–388.
- [6] O. Regev, Y. Cohen, E. Kehat, Y. Talmon, *Zeolites* **1994**, *14*, 314–319.
- [7] R. W. Corkery, B. W. Ninham, *Zeolites* **1997**, *18*, 379–386.
- [8] W. H. Dokter, H. F. van Garderen, T. P. M. Beelen, R. A. van Santen, W. Bras, *Angew. Chem.* **1995**, *107*, 122–125; *Angew. Chem. Int. Ed. Engl.* **1995**, *34*, 73–75.
- [9] S. Mintova, N. H. Olson, T. Bein, *Angew. Chem.* **1999**, *111*, 3405–3408; *Angew. Chem. Int. Ed.* **1999**, *38*, 3201–3204.

- [10] a) C. E. A. Kirschhock, S. P. B. Kremer, J. Vermant, G. V. Tendeloo, P. A. Jacobs, J. A. Martens, *Chem. Eur. J.* **2005**, *11*, 4306–4313; b) C. E. A. Kirschhock, V. Buschmann, S. Kremer, R. Ravishankar, C. J. Y. Houssin, B. L. Mojet, R. A. van Santen, P. J. Grobet, P. A. Jacobs, J. A. Martens, *Angew. Chem.* **2001**, *113*, 2707–2710; *Angew. Chem. Int. Ed.* **2001**, *40*, 2637–2640.
- [11] W. Fan, M. O'Brien, M. Ogura, M. Sanchez-Sanchez, C. Martin, F. Meneau, K. Kurumada, G. Sankar, T. Okubo, *Phys. Chem. Chem. Phys.* **2006**, *8*, 1335–1339.
- [12] a) T. P. Caremans, C. E. A. Kirschhock, P. Verlooy, J. S. Paul, P. A. Jacobs, J. A. Martens, *Microporous Mesoporous Mater.* **2001**, *90*, 62–68; b) A. L. Yonkeu, G. Mieke, H. Fuess, A. M. Goossens, J. A. Martens, *Microporous Mesoporous Mater.* **2006**, *96*, 396–404; c) R. J. Francis, S. J. Price, S. O'Brien, A. M. Fogg, D. O'Hare, T. Loiseau, G. Férey, *Chem. Commun.* **1997**, 521–522.
- [13] a) P. C. M. M. Magusin, V. E. Zorin, A. Aerts, C. J. Y. Houssin, A. L. Yakovlev, C. E. A. Kirschhock, J. A. Martens, R. A. van Santen, *J. Phys. Chem. B* **2005**, *109*, 22767–22774; b) B. H. Chen, Y. N. Huang, *J. Am. Chem. Soc.* **2006**, *128*, 6437–6446.
- [14] S. Mintova, N. H. Olson, T. Bein, *Science* **1999**, *283*, 12–14.
- [15] R. J. Francis, D. O'Hare, *Dalton Trans.* **1998**, 3133–3148.
- [16] V. P. Valtchev, K. N. Bozhilov, *J. Am. Chem. Soc.* **2005**, *127*, 16171–16177.
- [17] S. A. Pelster, R. Kalamajka, W. Schrader, F. Schüth, *Angew. Chem.* **2007**, *119*, 2349–2352; *Angew. Chem. Int. Ed.* **2007**, *46*, 2299–2302.
- [18] J. M. Shi, M. W. Anderson, S. W. Carr, *Chem. Mater.* **1996**, *8*, 369–375.
- [19] P. Norby, *J. Am. Chem. Soc.* **1997**, *119*, 5215–5221.
- [20] M. G. O'Brien, A. M. Beale, C. Richard, A. Catlow, B. M. Weckhuysen, *J. Am. Chem. Soc.* **2006**, *128*, 11744–11745.
- [21] G. Xiong, C. Li, H. Li, Q. Xin, Z. Feng, *Chem. Commun.* **2000**, 677–678.
- [22] C. Li, G. Xiong, Q. Xin, J. Liu, P. Ying, Z. C. Feng, J. Li, W. Yang, Y. Wang, G. Wang, X. Liu, M. Lin, X. Wang, E. Min, *Angew. Chem.* **1999**, *111*, 2358–2360; *Angew. Chem. Int. Ed.* **1999**, *38*, 2220–2222.
- [23] J. Twu, P. K. Dutta, C. T. Kresge, *J. Phys. Chem.* **1991**, *95*, 5267–5271.
- [24] F. Roozeboom, H. E. Robson, S. S. Chan, *Zeolites* **1983**, *3*, 321–328.
- [25] J. L. Guth, P. Caullet, P. Jacques, R. Wey, *Bull. Soc. Chim. Fr.* **1980**, *121*, 3–4.
- [26] J. Twu, P. K. Dutta, C. T. Kresge, *Zeolites* **1991**, *11*, 672–679.
- [27] P. McMillan, *Am. Mineral.* **1984**, *69*, 622–644.
- [28] D. W. Maston, S. K. Sharma, J. A. Philpotts, *Am. Mineral.* **1986**, *71*, 694–704.
- [29] P. K. Dutta, D. C. Shieh, M. Puri, *J. Phys. Chem.* **1987**, *91*, 2332–2336.
- [30] D. A. McKeown, F. L. Galeener, J. Brown, *J. Non-Cryst. Solids* **1984**, *68*, 361–378.
- [31] P. K. Dutta, D. C. Shieh, *J. Phys. Chem.* **1986**, *90*, 2331–2334.
- [32] G. Xiong, Y. Yi, Z. C. Feng, Q. Xin, F. S. Xiao, C. Li, *Microporous Mesoporous Mater.* **2001**, *42*, 317–323.
- [33] T. T. Trinh, A. P. J. Jansen, R. A. van Santen, *J. Phys. Chem. B* **2006**, *110*, 23099–23106.
- [34] M. J. Mora-Fonz, C. R. A. Catlow, D. W. Lewis, *Angew. Chem.* **2005**, *117*, 3142–3146; *Angew. Chem. Int. Ed.* **2005**, *44*, 3082–3086.
- [35] C. R. A. Catlow, D. S. Coombes, D. W. Lewis, J. C. G. Pereira, *Chem. Mater.* **1998**, *10*, 3249–3256.

Received: March 27, 2008  
Published online: April 21, 2008